ATTRIBUTE ANALYSIS OF ELECTROMAGNETIC WAVES IN DIFFERENT MEDIUMS USING GROUND PENETRATING RADAR

IFFAH ZALIKHA BINTI ROSLAN

UNIVERSITI SAINS MALAYSIA

2022

ATTRIBUTE ANALYSIS OF ELECTROMAGNETIC WAVES IN DIFFERENT MEDIUMS USING GROUND PENETRATING RADAR

by

IFFAH ZALIKHA BINTI ROSLAN

Thesis submitted in fulfilment of the requirements
for the Degree of
Master of Science

September 2022

ACKNOWLEDGEMENT

In the name of Allah, the Most Gracious, Most Merciful. Praise to Allah, peace and blessings of Allah upon His Messenger, Muhammad S.A.W., his family and companions. Alhamdulillah, first and foremost, praise Allah for His blessings and guidance in providing me with the patience and strength to complete the degree of Master of Science.

I would like to express my deepest appreciation to my main supervisor, Dr. Nur Azwin Binti Ismail, for her encouragement, patience, advice, and continuous support in completing my thesis report. Additionally, I would like to express gratitude to the Fundamental Research Grant [grant numbers FRGS/1/2018/STG09/USM/02/2] for funding this research. Moreover, I am grateful to the Institute of Postgraduate Studies at USM for funding my master's degree through the Fellowship program.

A great thanks to all Geophysics lab assistants for supporting this project by providing facilities and sharing their skills and experiences. Additionally, I would like to express my gratitude to my colleague for their invaluable contributions to geophysics field data acquisition and for sharing their knowledge and experiences for this project.

Countless thanks to my beloved parents Roslan Bin Haron and Hamimah Binti Haron as well as my sister Izzah Syafina Binti Roslan. Their prayers and support have benefited and motivated me greatly throughout the time I worked on my thesis.

Last but not least, I want to thank me. I want to thank me for believing in me. I want to thank me for doing all this hard work. I want to thank me for having no days off. I want to thank me for never quitting. I made it!

TABLE OF CONTENTS

LIST OF TABLES

Page

LIST OF FIGURES

Page

LIST OF SYMBOLS

A	Radius of the footprint area
$\vec{B}$	Magnetic flux density vector
c_0	Electromagnetic wave velocity in a vacuum
cm	Centimeter
d	Depth
$\vec{D}$	Electric displacement vector
ΔD	Distance between the two interfaces
$\vec{E}$	Electric field strength vector
f	Frequency
ft	Feet
F/m	Farads per meter
GHz	Giga hertz
$\vec{H}$	Magnetic field intensity vector
H/m	Henrys per meter
in	Inch
$\vec{J}$	Electric current density vector
K	Layer
km	Kilometer
m	Meter
mm	Millimeter
MHz	Mega hertz
m/s	Meter per second
m/ns	Meter per nanosecond
ns	Nanosecond
q	Electric charge density
S/m	Siemens per meter
t	Time

μ	Magnetic permeability
v	Velocity
σ	Electrical conductivity
ω	Angular frequency
π	Pie
Δ_v	Horizontal resolution
λ	Wavelength
ε	Dielectric permittivity
ε_0	Dielectric permittivity of vacuum space
ε_r	Relative permittivity
ε_{r1}	Relative permittivity of the first medium
ε_{r2}	Relative permittivity of the second medium
ε_{r3}	Relative permittivity of the third medium
$\overset{\frown}{v}$	Hyperbola/ diffraction fitting
$\times$	Multiplication
%	Percentage
$>$	Bigger - than
$<$	Less - than
$\sim$	Almost equal
$\pm$	Plus - minus
$^\circ$	Degree

LIST OF ABBREVIATIONS

CPT	Corrugated plastic tubing
E	East
EM	Electromagnetic
F-K	Frequency-wavenumber
G	Grave
GPR	Ground penetrating radar
Kya	Thousand years ago
N	North
NE	North East
NW	North West
PVC	Polyvinyl chloride
USM	Universiti Sains Malaysia
P	Pipe
R	Receiver antenna
RC	Reflection coefficient
S	South
SE	South East
SW	South West
T	Transmitter antenna
TDR	Time domain reflectometry
W	West
1-D	One dimensional
2-D	Two dimensional
3-D	Three dimensional

LIST OF APPENDICES

ANALISIS ATRIBUT GELOMBANG ELEKTROMAGNETIK DALAM MEDIUM YANG BERBEZA MENGGUNAKAN RADAR TUSUKAN BUMI

ABSTRAK

Radar tusukan bumi (GPR) telah digunakan secara meluas untuk mengesan ciri geologi subpermukaan cetek dan objek tertimbus buatan manusia seperti utiliti dan struktur arkeologi. Adalah kritikal untuk mentafsir data GPR dengan teliti untuk memberikan tafsiran yang boleh dipercayai bagi struktur permukaan cetek, kerana sebahagian jenis objek yang tertimbus sering menjana isyarat pantulan GPR yang sama. Oleh itu, penyelidikan ini bertujuan untuk mengenal pasti faktor-faktor yang mempengaruhi perambatan gelombang elektromagnetik (EM) di subpermukaan menggunakan GPR dan untuk menganalisis atribut gelombang EM dalam beberapa media dan geometri tinjauan serta untuk menghasilkan garis panduan asas kepada pengguna GPR dalam mentafsir data GPR. Pemerolehan data dalam kajian ini dibahagi kepada dua bahagian 1) model eksperimen dan 2) kajian lapangan. Pada kajian model eksperimen, isyarat gelombang radar dengan geometri objek yang berbeza-beza disiasat. Keputusan menunjukkan bahawa apabila lapisan/medium atas mempunyai ketelusan relatif yang lebih rendah daripada lapisan/medium di bawahnya, kekutuban adalah normal. Sebaliknya, apabila kekutuban pantulan diterbalikkan ia dipantulkan daripada bahan yang mempunyai ketelusan relatif yang lebih rendah daripada bahan di atasnya. Lebih besar kontras ketelusan relatif, lebih besar pekali pantulan, dan dengan itu lebih mudah untuk menggambarkan lapisan dan menemui ciri bawah permukaan. Pekali pantulan untuk kualiti kontras pemantulan telah dibahagikan kepada lemah (<0.3), baik (0.3-0.5) dan cemerlang (>0.5). Objek dalam

medium halaju rendah di sekeliling menghasilkan hiperbola sempit dengan tindak balas pantulan amplitud rendah sementara hiperbola luas dengan pantulan amplitud yang kuat ialah apabila kontras ketelusan relatif antara bahan kandungan terisi dan bahan sekeliling adalah tinggi. Pantulan amplitud terkuat dengan hiperbola paling sempit dihasilkan oleh orientasi antena bersudut tepat dengan objek, manakala antena selari dengan objek menghasilkan pantulan lurus dengan tindak balas pantulan amplitud rendah. Objek yang lebih dalam mencipta hiperbola luas dengan pantulan amplitud rendah. Ia juga diperhatikan bahawa apabila jarak antara objek adalah lebih kecil daripada resolusi frekuensi, kedua-dua objek antara dua permukaan tidak dapat diselesaikan. Selain itu, beberapa kajian berkaitan dengan arkeologi telah dijalankan di tanah perkuburan Permatang Pasir dan Titi Teras, bidang geologi di Guar Kepah, dan bidang kejuruteraan di kampus USM. Tiga umur pengebumian berbeza ditemui di kawasan perkuburan (muda, pertengahan dan tua) sementara tiga jenis tanah dan saiz bijirin yang berbeza ditemui di kawasan Guar Kepah. Kajian utiliti di kampus USM menemui dua jenis paip dengan pelbagai bahan penutup dan kandungan isi. Atribut isyarat daripada model eksperimen digunakan dalam tafsiran keputusan kajian kerja lapangan GPR. Garis panduan ukuran yang dihasilkan akan membantu pengguna akhir dalam membentuk tinjauan GPR dan mentafsir isyarat GPR dengan input asas mengenai atribut GPR.

ATTRIBUTE ANALYSIS OF ELECTROMAGNETIC WAVES IN DIFFERENT MEDIUMS USING GROUND PENETRATING RADAR

ABSTRACT

Ground-penetrating radar (GPR) has been widely used to detect shallow subsurface geological features and man-made buried objects such as utilities and archaeological structures. It is critical to interpret GPR data thoroughly to provide reliable interpretations of near-surface structures, as certain types of buried objects frequently generate similar GPR reflection signals. Thus, this research aims to identify the factors affecting electromagnetic wave (EM) propagation in the subsurface using GPR and to analyze the EM wave attribute in several media and survey geometry as well as to produce a basic guideline for GPR practitioners in interpreting the GPR data. The data acquisition in this study is divided into two parts; 1) experimental model and 2) field study. In the experimental model, radar-wave signals were investigated with varying object geometry. Results indicated that when the upper layer/medium had a lower relative permittivity than the layer/medium underneath, the polarity is normal. By contrast, the reflection polarity is reversed when it is reflected from a material with a lower relative permittivity than the material above it. The greater the relative permittivity contrast, the greater the reflection coefficient, and hence the easier it is to delineate layers and discover subsurface features. The reflection coefficient of reflectivity contrast quality is divided into weak (<0.3), good (0.3-0.5) and excellent (>0.5). The object in the surrounding low-velocity medium produced a narrow hyperbola with a low amplitude reflection response while the broad hyperbola with strong amplitude reflection is produced when the relative permittivity

contrast between filled content and surrounding medium material is higher. The strongest amplitude reflection with the narrowest hyperbola is produced by the antenna orientation perpendicular to the object, while the antenna parallel to the object produced linear reflection with a low amplitude reflection response. A deeper object created a broad hyperbola with a low amplitude reflection. It was also observed that when the object's interface distance is smaller than the frequency's resolution, both interfaces remain unresolved. In addition, several field studies related to archaeology were conducted in Permatang Pasir and Titi Teras cemetery, the geological field in Guar Kepah, and the engineering field in the USM campus. Three different burial ages were discovered in the cemetery areas (young, intermediate and old) while three different types of soil and grain sizes were discovered in Guar Kepah. A utility study at the USM campus discovered two types of pipes with varies covering materials and filled content. The signal attributes from experimental models were utilized in the interpretation of GPR field study results. The standard guideline produced will assist the end-user in designing a GPR survey and interpreting the GPR signals with basic input regarding the GPR attribute.

CHAPTER 1

INTRODUCTION

1.1 Preface

Ground penetrating radar (GPR) is one of the most popular geophysical approaches to locate and detect shallow subsurface objects because it offers high-resolution images. The transmitting antenna transmits an electromagnetic (EM) pulse into the ground, which is partially reflected when it comes into contact with material with varying electrical properties and partly transmitted into deeper layers. A receiving antenna then records the reflected signal (Neal, 2004). A variety of factors can influence the EM pulses during transmission and reflection. During field measurements, misinterpretations in subsurface material identification are frequently caused by numerous noise sources from non-dominant/inhomogeneous materials. Inhomogeneity in a medium occurs due to variations in conductivity, relative permittivity, and magnetic permeability properties caused by the media's varied composition (Arisona et al., 2017). Thus, understanding the target's and medium's properties is critical for proper GPR signal interpretation or analysis. In addition, the soils are commonly considered to be non-magnetic. However, this isn't the case if they include high amounts of magnetic minerals like iron oxides (Curioni et al., 2017). Thus, the EM characteristic of non-magnetic soils can be labeled by the electrical properties only (relative permittivity and electrical conductivity). Besides, the electrical properties of the medium may vary according to conditions in the soil, affecting GPR signals during the GPR survey.

Another distinct advantage of GPR is its potential for defining the size, shape, depth, orientation and separation of buried objects. Buried targets produce hyperbolic signatures in the radargram obtained by moving the GPR system crossing the target. The size, shape, and dielectric properties of the target and the orientation of the electric field are all represented as different hyperbolic signatures (Dou et al., 2017). The difficulties arise in detecting and classifying targets in an environment with variations in the surface cover such as soil, grass, sand, asphalt and concrete. In addition, the subsoil with spatial vertical or horizontal variability in the soil texture such as multilayer, different water content and backfill soil will also cause some problems in discovering the target using the GPR system. In the presence of buried targets which is close to one another and have variation material, for example, one is metal and another is non-metal, they are sometimes undetectable by the GPR.

Detailed subsurface interpretation is critically important to provide a reliable interpretation of near-surface structures. This allows to characterize and analyze the GPR capability to detect and distinguish objects such as piping among different types or objects. Therefore, GPR signal analysis must be addressed in order to assist users with data interpretation and minimize misinterpretation. This thesis examines the GPR signals on the various object geometries and medium to determine their signals based on their hyperbolic and amplitude reflection behaviors.

1.2 Problem Statement

GPR is a non-invasive geophysical method for detecting electrical discontinuities in the subsurface. Detailed subsurface interpretation is critically important to provide a

reliable interpretation of near-surface structures in the different medium backgrounds. However, without a good understanding of the signature governing this response, GPR results can easily be misinterpreted. First, a previous study stated that the positions of antenna, depth or size of the buried object could generate a hyperbola curve. Some conflicts arise to interpret and differentiate the size and behavior of the hyperbola curve when it crosses those factors. Besides, the GPR signal can vary across the reflecting media depending on the relative permittivity contrast between media. The conflicts arise when determining the surrounding medium and filling medium type. In this case, a thorough understanding of the reflection coefficient and polarity used to generate the images within a geological environment will result in an accurate final result. Therefore, it is critical to interpret GPR signals thoroughly to provide reliable interpretations of near-surface structures, as certain underground objects frequently generate similar GPR reflection data.

1.3 Research Objective

The objectives are divided into the following points:

1. To identify the factors affecting electromagnetic waves (EM) propagation in the subsurface using GPR.
2. To analyze the EM wave attribute in several media and survey geometry.
3. To produce a basic guideline for GPR practitioners in interpreting the GPR data.

1.4 Scope of the study

The scopes of the study focus on different medium using GPR and the fine points are as follow:

1.4.1 Experimental model

The experimental model is designed to simulate a range of potential configurations of different buried objects with varying coverings that closely mimic the most frequently encountered field studies. The study examines radar-wave signals with varying depths, mediums, object materials, filled contents, diameter, orientation, and overlapping in horizontal and vertical directions to characterize and explore their ability to detect, locate, and differentiate various buried objects. In addition, different GPR signatures (reflection coefficient, polarity, and reflection behavior) were analyzed to ensure an effective field data interpretation that yields accurate detection results.

1.4.2 Field study

The series of buried objects and stratigraphy layers were also estimated in uncontrolled field conditions using knowledge of the signal behavior at the experimental scale. Although the object on the field settings and the model in this study were different, the fundamental response characteristics were similar. Fieldwork was conducted in archaeological, geological, and engineering areas. These sites include various geologic materials and underground objects/utilities, resulting in various GPR reflection signals. This section shows the results of detailed 1-D, 2-D and 3-D GPR surveys.

1.5 Significant of the study

This research aims to develop controlled models for estimating the GPR signature using controlled details of subsurface structure. Numerous subsurface structures were analyzed in this study, including object diameters, materials, filled contents, orientation,

burial depth, burial medium, and target overlapping in both horizontal and vertical directions on the radar-wave signal, to determine the GPR signature and provide accurate reflection signal interpretation. Variation in hyperbola behavior was generated due to the effects of subsurface structures in this study. Additionally, the reflection coefficient is a hugely important signature for evaluating the contrast between the target and the surrounding medium. Similarly, the polarity traces will aid in understanding the physical properties (relative permittivity) of the ground materials that produce reflections. Classifying those subsurface structures using these GPR signatures is important for validating their correct location. This research will help GPR practitioners, educators, and researchers to discover more about the GPR signal's behavior towards the non-homogenous subsurface and assist in designing GPR survey and interpreting the GPR signals with basic input regarding the GPR attribute.

1.6 Layout of thesis

The thesis comprises five chapters and is outlined briefly as follows:

Chapter 1 is an introductory chapter that summarizes the research context by highlighting the electromagnetic wave parameters in various mediums using GPR. This chapter discusses problem statements, research objectives, the scope and significance of the study. Additionally, the framework of the thesis is also discussed here.

Chapter 2 reviews the literature on GPR theory, the GPR field system, and previous research. Previous research has been based and deliberated on two areas: identifying the site's condition and the signatures used in GPR. There are six primary considerations when determining the condition of a site: the medium type, the object material, the filled contents,

the object diameter, the object orientation, and the object depth. In addition, the GPR signatures discussed in this section are the hyperbola behavior, the reflection coefficient, and the polarity response.

Chapter 3 detailed the workflow of the study and divided it into two main parts. The first section discusses how the experimental model is used to generate preliminary results and model a variety of possible configurations of various buried structures that closely mimic the most commonly observed in field studies. The second section went into detail on how the real site data was performed. The same procedure for the experimental model was used at the real site.

Chapter 4 addresses the study results, including data analysis, interpretation, and discussion. It involves the interpretation of an experimental model and a field study's data. This chapter explains the experimental model's findings, which can be used as a reference for field study analysis. As a result, to prove the method's effectiveness and capability, the model and field study findings are compared and discussed.

Chapter 5 summarizes the major findings of this research and provides recommendations for future research to provide improvements in the years to come.

CHAPTER 2

LITERATURE REVIEW

2.1 Introduction

GPR is a non-destructive method of searching for subsurface anomalies. GPR uses the EM field theory, which is based on Maxwell equations. GPR works by sending EM energy into material from a transmitter antenna. The antenna recorded the amplitude and travel time of the received signal. The constitutive equations determine the reflected signal response, which is used to interpret the target features. Understanding GPR signal response and performance requires a study of the GPR concept and radar parameters.

The second chapter is divided into three sections. First is the theory of GPR. The second section describes the GPR field system and the last section describes the researchers' previous research on the site conditions and radar signatures. The last section will also cover how to use the information gathered by the user to generate suggestions that will aid in discovering buried anomalies using GPR.

2.2 Basic GPR concept

2.2.1 Generation of electromagnetic wave

The GPR signal is based on Maxwell's equations, which explain the propagation of electromagnetic waves in a medium mathematically (Annan, 2003). The following is a quantitative description of the relationship between EM properties and EM wave propagation:

$$\nabla \times \vec{E} = -\frac{\partial(\vec{B})}{\partial t} \quad (2.1)$$

$$\nabla \times \vec{H} = \vec{J} + \frac{\partial(\vec{D})}{\partial t} \quad (2.2)$$

$$\nabla \times \vec{D} = q \quad (2.3)$$

where $\vec{E}$ is the electric field strength vector, $\vec{B}$ is the magnetic flux density vector, $\vec{D}$ is the electric displacement vector, $\vec{H}$ is the magnetic field intensity vector, $\vec{J}$ is electric current density vector, q is the electric charge density and t is time. Equations 2.4, 2.5 and 2.6 are a compilation of electric current density, electric current displacement, and magnetic flux density vectors, respectively, known as the constitutive equations. These are the following:

$$\vec{J} = \sigma\vec{E} \quad (2.4)$$

$$\vec{D} = \varepsilon\vec{E} \quad (2.5)$$

$$\vec{J} = \mu\vec{E} \quad (2.6)$$

where σ is electrical conductivity in S/m, ε is relative permittivity in F/m, and μ is magnetic permeability in H/m. These three physical properties control how the EM wave propagates through the material (Annan, 2003).

The conductivity and magnetic permeability of a propagating wave determines its attenuation. For example, clay-rich or saline conditions (high conductivity and electrical loss) attenuate EM signals. On the other hand, magnetic permeability is normally only considered in magnetic ore bodies and is assigned a value corresponding to nonmagnetic materials (μ= 1). Since the GPR is often used in low-loss materials, the effect of conductivity and magnetic permeability is negligible (Baker et al., 2007). As a result, the key property controlling the propagation velocity of an EM wave is relative permittivity. Relative permittivity determines a material's ability to store and release EM energy in the

form of an electric charge which can be calculated in situ or in the lab (Baker et al., 2007). The relative permittivity, conductivity, and EM velocity for selected materials are shown in Table 2.1.

Table 2.1 EM velocity and relative permittivity for selected materials (Davis & Annan, 1989; Hammon et al., 2000; Neal, 2004; Baker et al., 2007; Cassidy, 2009; Damiata et al., 2013; Rodrigues et al., 2021).

Materials	Relative permittivity (ε_r)	Velocity (m/ns)	Conductivity (S/m)
Air	1	0.3	0
Asphalt	3 - 5	0.173 – 0.134	Not available
Clay - dry	2 - 20	0.09 – 0.12	0.001 – 0.1
Clay - wet	15 - 40	0.05 – 0.07	0.1 - 1
Concrete - dry	4 - 10	Not available	0.001 – 0.01
Concrete - wet	10 - 20	Not available	0.01 – 0.1
Freshwater	80	0.03	0.0001 – 0.01
Metal	Not available	Not available	1×10^{6}
Human - bones	5-13	Not available	0.1
Human – liver, muscle, lung	49	Not available	0.75
Sand – dry	3 – 6	0.1 – 0.2	1×10^{-7} – 0.001
Sand - wet	10 – 30	0.05 – 0.08	0.0001 – 0.01
Sand – coastal, dry	5 -10	Not available	0.00001 – 0.001
Seawater	80	0.01	30
Soil – sandy, dry	4 – 6	0.12 – 0.15	0.0001 – 0.1
Soil – sandy, wet	15 – 30	0.05 – 0.08	0.01 – 0.1
Soil – clayey, dry	4 – 6	0.12 – 0.15	0.0001 – 0.1
Soil – clayey, wet	10 -15	0.08 – 0.09	0.1 - 1
Soil – loamy, dry	4 – 6	0.05 – 0.08	0.0001 – 0.001
Soil – loamy, wet	10 - 20	0.07 – 0.09	0.01 – 0.1
PVC	3	0.173	0.001
Wood	2-3	Not available	Not available

2.2.2 Propagation of EM waves in dielectrics

The propagation of EM waves through a medium is characterized by the EM properties of the medium, such as relative permittivity (ε_r), conductivity (σ) and magnetic

permeability (μ). In a host medium, the propagation velocity, v, can be measured as follows (Annan, 2003):

$$v = \frac{c_0}{\sqrt{\varepsilon_r \mu \frac{1+\sqrt{1+(\frac{\sigma}{\omega\varepsilon})^2}}{2}}} \quad (2.7)$$

where c_0 is the electromagnetic wave velocity in a vacuum (3 x 10^8 m/s), $\varepsilon = \varepsilon_r \times \varepsilon_0$ is the dielectric permittivity ε_0 is the dielectric permittivity of vacuum space (8.854 x 10^{-12} F/m), $\omega = 2\pi f$ is the angular frequency (rad s^{-1}) where f is frequency, and the expression $\sigma/\varepsilon\omega$ is a loss factor (Annan, 2003).

In loss material, where $\sigma/\varepsilon\omega = 0$ (Davis & Annan 1989), the velocity of the EM wave is simplified to the expression:

$$v = \frac{c_0}{\sqrt{\varepsilon_r}} \quad (2.8)$$

When the velocity is known, the depth of an object or interface, d can be estimated by:

$$d = \frac{vt}{2} \quad (2.9)$$

where t is the two-way travel time of the radar signal from the antenna to the reflection point and back to the antenna.

2.2.3 Reflection coefficient

The reflection coefficient equation can predict the GPR response based on where the reflection will occur and what it will reveal. The reflection coefficient (RC) determines the percentage of energy reflected with signal amplitude. Assuming that σ and μ are both negligible, the RC ratio can be expressed numerically as follows:

$$RC = \frac{(\sqrt{\varepsilon_{r2}} - \sqrt{\varepsilon_{r1}})}{(\sqrt{\varepsilon_{r2}} + \sqrt{\varepsilon_{r1}})} \quad (2.10)$$

where ε_{r1} and ε_{r2} are the relative permittivity of the upper and lower medium, respectively. The RC equation determines the GPR response. It allows for the calculation at the interface of reflected energy and can give data regarding signal polarity. The positive and negative of the reflection polarity are determined by the permittivity contrast between two media at the interface (Neal, 2004; Annan, 2003).

2.2.4 Resolution

The two types of resolution shown in Figure 2.1 are vertical (down-range, depth or longitudinal) resolution (Δ_v) and horizontal (cross-range, angular or lateral) resolution (Δ_H) using the transmitter antenna (T) and receiver antenna (R).

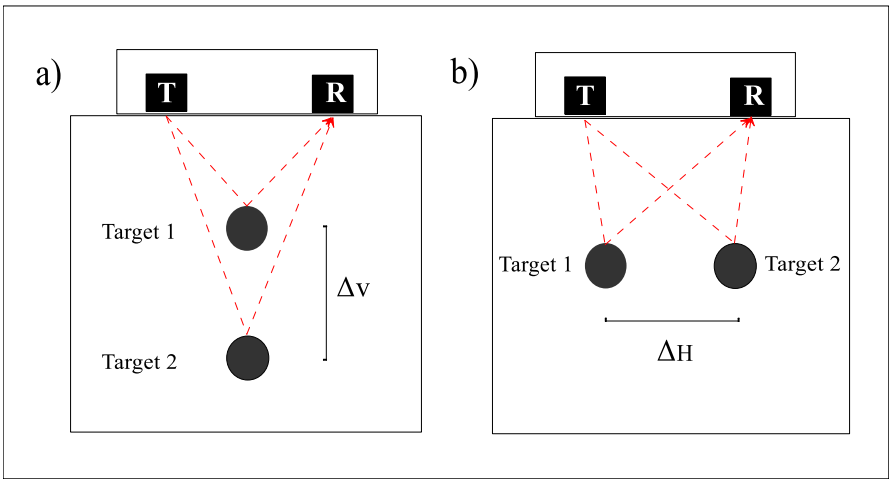

Figure 2.1 Schematic representation of a) vertical and b) horizontal resolutions.

2.2.4(a) Vertical resolution

There are two different meanings of resolution in seismic reflection (Knapp, 1990). These can be applied directly to radar data. The first is the ability to identify the location of a reflector in space or time. The wavelet sharpness or pulse width is a factor in vertical resolution. Vertical resolution is proportional to frequency according to this term.

Therefore, vertical resolution increases with frequency (Knapp, 1990) (Figure 2.2). The second principle of resolution is the ability to resolve two closely separated features (Leucci et al., 2003; Rial et al., 2009) (Figure 2.1a). Wave theory suggests that the best vertical resolution can reach one-quarter EM wave wavelength (Annan, 2003). Wavelength (λ) is the direct function of the wave frequency (f) and propagation velocity (v):

$$\lambda = \frac{v}{f} \tag{2.11}$$

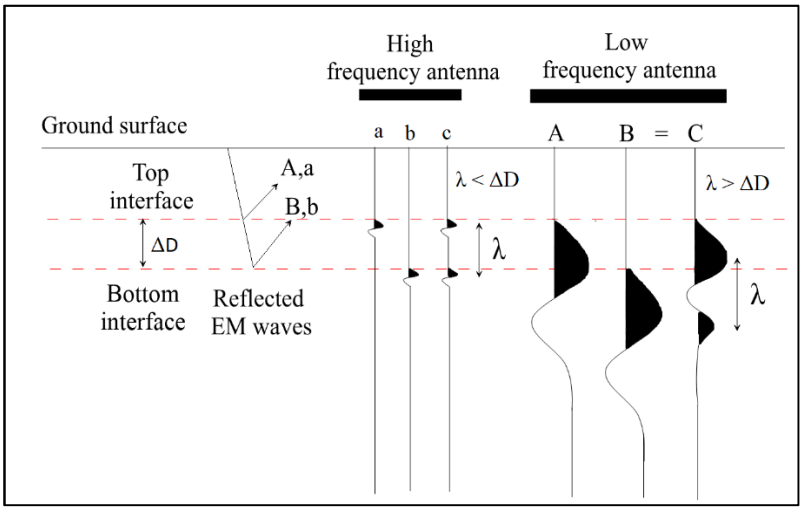

Figure 2.2 The resolution and penetration depth of GPR antennas operating at high and low frequencies. A high-frequency EM wave defines both the top (a) and bottom (b) interfaces. The resulting wave (c) will resolve both interfaces if it is less than the distance between the two interfaces (ΔD). The top interface is defined by a low-frequency wave (A), but the distance between the interfaces (ΔD) is smaller than the wavelength (B). Both interfaces will remain unresolved due to the comparatively long-wavelength (λ) of the resulting EM signal (C). However, the penetration depth is greater in this situation than with a high-frequency antenna (after Buynevich et al., 2008).

2.2.4(b) Horizontal resolution

A GPR transmitting antenna generates energy in the form of a beam that travels in an elliptical cone downward into the earth (Figure 2.3). The radius of the cone extends as the penetration depth increases, resulting in a wider footprint scanned underneath the antenna (Neal, 2004). The formula may be used to estimate the footprint area.

$$A = \frac{\lambda}{4} + \frac{D}{\sqrt{\varepsilon+1}} \quad (2.12)$$

where A is the radius of the footprint area at depth D, λ is the antenna's central frequency wavelength, and ε is the scanned materials' relative permittivity. Horizontal resolution refers to the shortest distance between two reflectors at the same depth (Gracia et al., 2008) (Figure 2.1b). This parameter is primarily determined by the trace interval manually adjusted before data acquisition and the reflector beam width and depth (Rial et al., 2009). The beam width is determined by the antenna's characteristics and the propagation medium. The higher the ability to resolve in discriminating adjacent targets, the narrower the beam width.

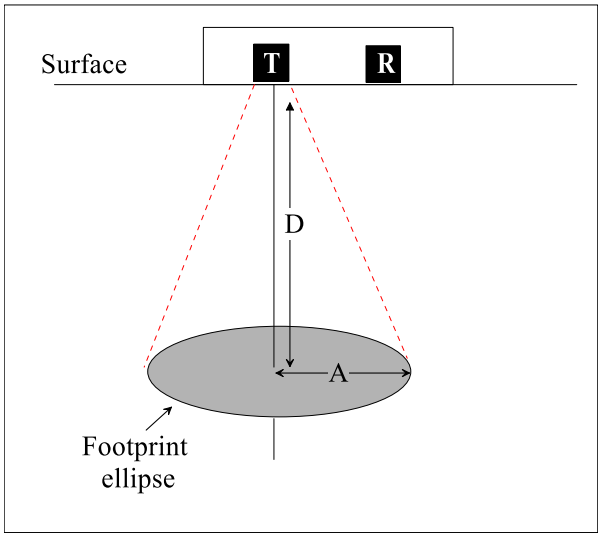

Figure 2.3 Scheme of the antenna footprint used to define the horizontal resolution.

2.3 GPR field system

2.3.1 GPR operation

A typical GPR system has an antenna that can transmit and receive signals with specific frequencies. The transmitting antenna radiates short pulses of the radio waves into

the field. The transmitted energy is reflected from various buried objects and contrast in relative dielectric permittivity. The receiver unit detects the reflected signals and is amplified and displayed by the control unit (Figure 2.4).

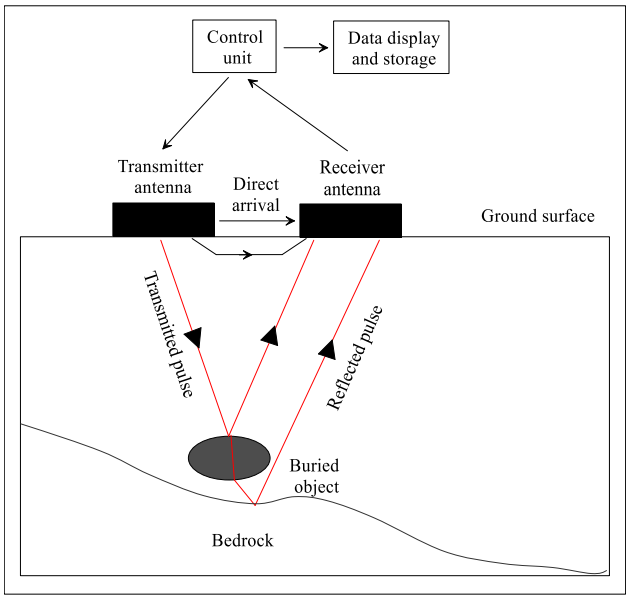

Figure 2.4 Schematic diagram principle of GPR.

2.3.2 GPR display

GPR data can be acquired and presented in three multiple formats. These GPR images are referred to as 1-D, 2-D and 3-D.

Figure 2.5 shows a sketch of the emitted and recorded signal in wiggle mode. The captured signal is referred to as a 1-D or a trace. Each reflection trace consists of a series of stacked waves received from certain depths in the ground at one surface location, varying in amplitude depending on the amount and intensity of energy reflection at buried interfaces. The 1-D image will aid in understanding the physical properties of ground materials that produce reflections. For instance, analyzing buried materials requires

understanding the polarity of waves recorded in individual reflection traces (Conyers, 2015).

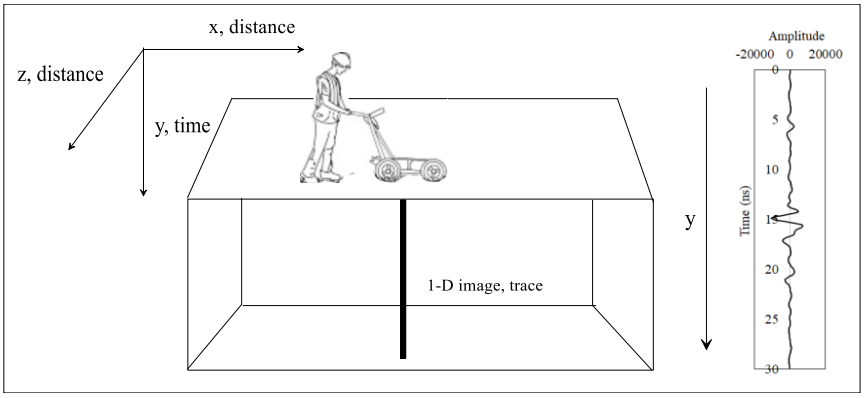

Figure 2.5 A single GPR measurement (1-D) generates a single time series at a single location.

The 2-D image or radargram shows the time of travel on the y-axis and spatial distance on the x-axis, a sequence of 1-D combined for a given spatial distance (Figure 2.6).

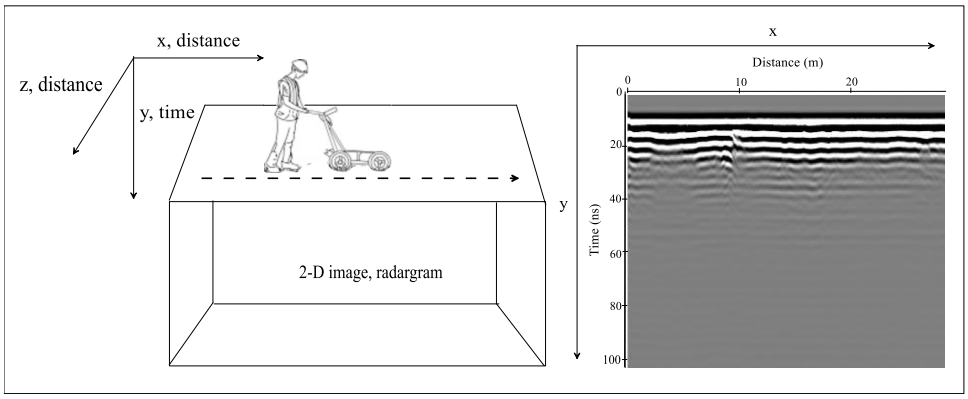

Figure 2.6 2-D data acquisition and display of a radargram.

The majority of the pattern forms used in radargram are hyperbolic curves or linear continuos reflection. Linear continuos reflection is caused by planar interfaces between layers with different electrical properties. However, hyperbolic curves are generated by point reflector (buried object) with cross-section sizes on the order of the radar pulse

wavelength (Mechbal & Khamlichi, 2014). Based on the reflection characteristics of an EM energy, the radar energy can be transmitted before and after the antenna is positioned over a point reflector. As the transmitter antenna approaches the point reflector, the propagation time measured at the receiving end decreases. As the antenna travels away from the target, the propagation time measured at the receiving end increases, resulting in a hyperbola curve (Figure 2.7). When the antenna is directly on top of the point reflector, the apex of the hyperbola indicates the precise location of the point reflector. The hyperbola's arms represent the reflected energy that travels in the oblique wave direction (Conyers, 2007). The hyperbola curve parameter can be obtained by fitting a curve to the hyperbola. The parameters can calculate each reflector's depth, size, and average EM wave velocity in the medium (Manataki et al., 2015; Dou et al., 2017).

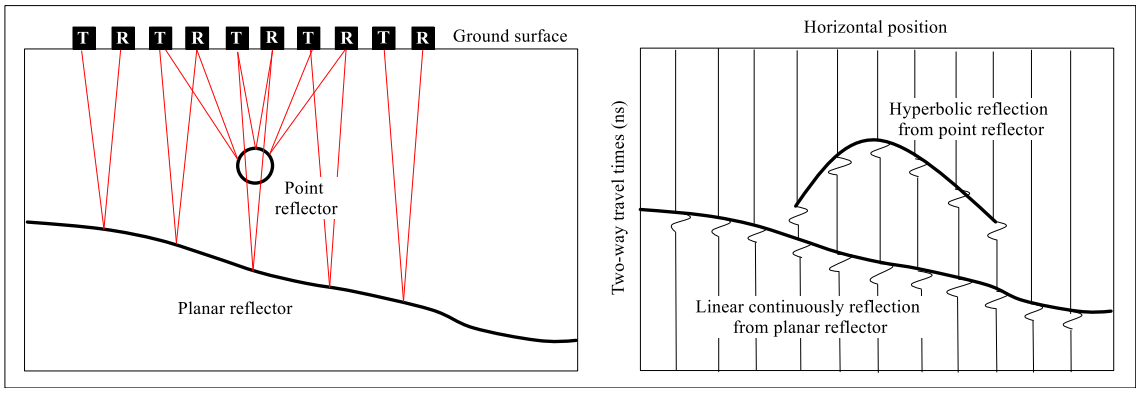

Figure 2.7 The planar and point reflectors are illustrated schematically with the formation of linear and hyperbolic reflections, respectively.

When many reflection profiles are collected in a grid, 3-D images of buried materials in the ground can be constructed (Figure 2.8). Time (or depth) slices are generated in this case. These slices are maps on which the reflection amplitudes have been projected at a certain time (or depth) and thickness (Conyers, 2015). These GPR slice maps are widely used because they display the depth evolution of buried structures and their scale,

shape, and position. Several publications go through the steps involved in creating 3-D images from GPR data (Bonomo et al., 2011; Jol et al., 2003; Hansen et al., 2014; Parmen et al., 2017). In addition, time or depth GPR slices improve imaging by detecting and interpreting subtle features that would otherwise be indistinguishable on radargrams (Ronen et al., 2019).

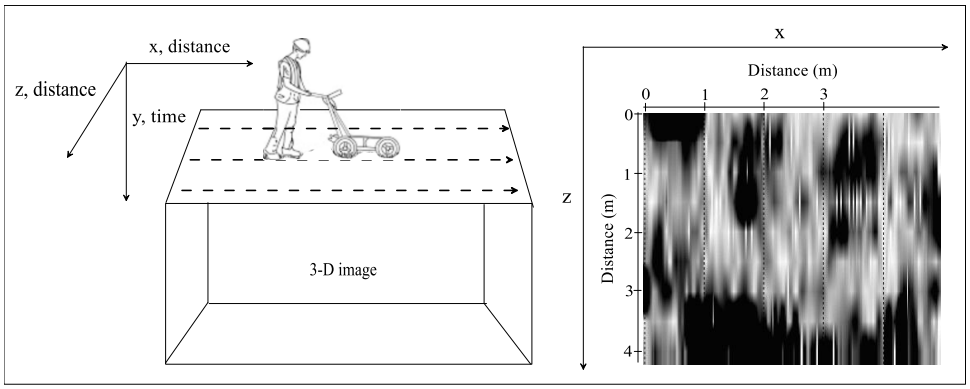

Figure 2.8 3-D data acquisition and display of a time slice.

2.4 Previous study

2.4.1 Site conditions

This section covers the information gathered by the practitioners to understand the site's conditions and assist in identifying buried anomalies using GPR.

2.4.1(a) Soil/ medium type

GPR data may also assess soil type because each soil has its geological composition, relative permittivity, and electrical conductivity properties (Saarenketo, 1998). Soil electrical conductivity is important in determining radar signal attenuation and penetration depth. In essence, as soil electrical conductivity increases, radar signal penetration decreases. Soil electrical conductivity is influenced by soil texture, salinity, and

moisture content. However, the propagation velocity of EM waves is determined by relative permittivity properties, which is the primary controlling factor in generating reflections (Baker et al., 2007).

Fine-grained material (e.g., clay and silt) has the greatest effect on GPR signals, causing substantial attenuation due to increased electrical conductivity percentage (Rogers et al., 2009). Fine-textured soils have a uniform appearance. In GPR profiles, Saarenketo and Scullion (2000) and Allred et al. (2018) found no ringing. This is due to the attenuation of propagated electromagnetic waves at silt/clay soil layers, reducing apparent resistivity or increasing electrical conductivity in the atmosphere while providing weaker GPR reflection (Afshar et al., 2015). Coarse-grained materials (e.g., gravel and sand) have lower electrical conductivity. As a result of the lower signal attenuation, they are often ideal conditions for GPR investigations (Saarenketo & Scullion, 2000; Allred et al., 2005; Aktürk & Doyuran, 2015). Coarse-grained soil with dielectric dispersion has a heterogeneous or cluttered appearance in the GPR profile (Saarenketo, 1998; Allred et al., 2018). This is because some highly reflective layers in sandy soil may be caused by thin beds of silty/clayey material with higher water-holding ability than the underlying coarse-grained sediments, resulting in dielectric constant discontinuities in the subsurface (Allred et al., 2005).

The soil morphology can also be seen in the GPR profiles. Chakraborty et al. (2019) used a 400 MHz antenna and discovered that the undisturbed soil body appeared homogeneous and continuous in the GPR profile because of the lack of contrast in relative permittivity characteristics. Meanwhile, any deformation of soil layer, including void formation, bending and soil layer sagging were easily interpretable in GPR profile because

non-homogeneous (Chakraborty et al., 2019). According to Rashed and Al-Garni (2013), the disturbed soil had a lower amplitude reflection than the surrounding area and rough discontinuous reflections.

2.4.1(b) Object material

GPR surveys successfully track underground objects such as metallic and non-metallic materials. Metallic materials shows strongest amplitude reflection in GPR profile due to the high dielectric contrast with soil (Chakraborty et al., 2019). This is because the vast majority (90%) of radar-wave energy was reflected from the top of metal material, with just less than 10% of energy penetrating the top of metal material. The radar-wave speed decreased after passing through the metal material because the transmitted energy was weak (Lee et al., 2013). Sutton et al. (2013) used GPR to detect the reflection of the top and bottom metal coffins, and their findings revealed multiple reflections in sandy soil environments. Metal multiples reflections are created as energy is reflected between metal objects within the casket's void space. It emits a "ringing" of energy from the reflection profile underneath the object. Other burials with only the top of the coffin covered in metal yield clear reflections but no multiple reflections. Previous utility investigations also have shown a high amplitude reflection from the metal pipe (Zeng & McMechan, 1997; Bonomo et al., 2011; Porsani et al., 2012; Rashed & Al-Garni, 2013).

On the other hand, non-metallic material reflection is significantly weaker to radar than metal material reflection (Chakraborty et al., 2019) and can be difficult to detect due to their reflective type (Bowders et al., 1982; Allred & Redman, 2010) . According to Lee et al. (2013), most radar-wave energies went through the non-metal pipes, with less than 10% reflected by the pipes' tops. As a consequence, the reflection revealed only very weak

signals. Since most of the energy (more than 90%) entered the non-metal pipes, the wave speed increased after the wave passed through the non-metal pipes. Experiments in the lab have demonstrated that the material's low dielectric properties such as PVC/non-metal tubing and human bones could be observed using GPR equipment (Zeng & McMechan, 1997; Hammon et al., 2000; Prego et al., 2017; Amran et al., 2018). However, the return signal from non-metallic materials is too weak to distinguish for practical purposes. According to Hammon et al. (2000), GPR responses on various buried body cross-sections are depends on the survey frequency, burial depths, soil types and moisture contents. Lower frequencies (450 MHz) could be utilized to identify burials in soils with significant moisture content or clay content. Meanwhile, high frequency (>900 MHz) could be used on dry or sandy soil environment and shallow burial depth. Zeng and McMechan (1997) found that the response of PVC or non-metal material object depends on the contrast between the surrounding soil and the contents of the object.

2.4.1(c) Filled contents

Differences in the dielectric properties across an object govern the amount of radar energy that reflects off the object and then returns to the surface to be recorded by the receiving antenna. Allred and Redman (2010) discovered that the non-metal drainage pipe response was determined by the contrast relative permittivity between the material found inside the pipe (air, water, or soil) and the surrounding soil, not by the form of pipe (clay tile or CPT). A field investigation conducted by Allred et al. (2005) gives further proof of this statement as the type of material covering the drainage pipe, either corrugated plastic tubing (CPT) or clay tile, has little impact on the GPR drainage pipe response but when filled with water shows a clear reflection when compared to the air-filled drainage pipe.

This is because of the similarity between the dielectric constant of pipe material and surrounding media. Bowders and Koerner (1982) also found that when the plastic drums were filled with water and salt, the plastic could be detected with clear reflection. The fresh water drum was slightly more noticeable than the salt water drum due to the fresh water's greater reflection potential. Meanwhile, the steel drums clearly showed reflection without filled material because of the high reflectivity. This study also showed a good agreement with the previous research conducted by Zeng and McMechan (1997), Chlaib et al. (2014), Koivisto et al. (2014), Conyers (2015).

2.4.1(d) Object diameter

Allred et al. (2005) point out that selecting the appropriate antenna frequency depending on the drainage pipe diameter is important. The author found that the 250MHz central frequency antennas appeared to be the most effective at detecting buried agricultural drainage pipe at depths up to 1 m (3 ft) and seem to be reasonably capable of detecting buried drainage pipes with diameters as small as 5 cm (2 in) in silty clay soil. However, antennas with a center frequency of 100MHz are the best choice for larger diameter pipes at greater depth (8-10 m) (Chakraborty et al. 2019). According to Kofman et al. (2005), two karst anomalies were discovered based on their scale and the relationship between size and frequency. The diffracting hyperbola for small while irregular signals with chaotic reflections for large sizes. Zeng and McMechan (1997) presented simulation findings on the diameter of tanks. The tanks are made of fiberglass filled with fresh water and buried in the silty clay with 1 m depth. The results show that as the tank diameter increases, so does the radius of curvature of the top and bottom reflections. Next, as the tank diameter increases, the reflections from the top and bottom become separated in time.

The tank size could be determined from the zero-offset time difference at the apex of the reflections if the tank contents are known (independent of the material in which the tank is buried).

2.4.1(e) Object orientation

Research by Radzevicius and Daniels (2000), Allred et al. (2005), Prego et al. (2017) provide indications that the orientation of the GPR survey line with the pipe orientation has a significant impact on the quality of the data collected. Specifically, Allred et al. (2018) conclude that when the antenna is moved perpendicular lines ($15° < x° < 90°$) to the pipe direction and the predicted pattern of reflection from the pipe is a hyperbola reflection. However, when the profile line is collected by moving the antenna parallel ($x° < 15^{o}$) to the pipe direction, the resulting reflection is a continuous flat reflection. When a flat reflection is formed, it is difficult to determine if it corresponds to a pipe, an interface between two separate layers of subsoil, or simply a reflection multiple. Other burial features, such as large stones, could also create a hyperbola of reflection, but their positions are separated by a map view, while the drainage pipe hyperbolas form a line (Allred et al. 2018).

According to Allred (2013), the strength of the GPR drainage pipe reflection was dependent on the orientation of the GPR antennas to the drain line for a particular soil moisture condition. The best GPR drainage pipe result was obtained when the clay loam soil was relatively dry and the GPR antenna was oriented perpendicular to the drain line. In contrast, a GPR antenna oriented parallel to a drain line offered the best GPR drainage pipe solution in extremely wet soil conditions. Radzevicius and Daniels (2000) also added that a GPR antenna orientation perpendicular to the buried cylinder would produce a

stronger GPR response than antenna orientation parallel to the buried cylinder for relatively small diameter cylinders buried beneath the ground surface where the cylinder's dielectric constant is substantially less than the dielectric constant of the surrounding soil. However, if the dielectric constant of the buried cylinder is significantly higher than the dielectric constant of the surrounding soil, a GPR antenna oriented parallel to the buried cylinder's axis would produce a stronger GPR response than an antenna oriented perpendicular to the buried cylinder's axis.

2.4.1(f) Object depth

The object's depth determines the shape of the hyperbola. This is because the GPR signal propagates with depth. A diffraction hyperbola with a deeper object would have a wider aperture diameter than a shallow object (Dondurur, 2018). According to Benedetto and Benedetto (2014), the time delay between reflections (i.e., the depth of the hyperbola's apex) is proportional to the object's depth. Additionally, selecting the appropriate antenna frequency depending on the subsurface depth of the buried target is important. The smaller the frequency, the greater the penetration depth of the radar signal. A low-frequency antenna of approximately 100 MHz is sufficient to collect data with acceptable resolution from less than 2 m to around 15 m depth. The penetration depth is limited to 2 m at higher frequencies (>400 MHz), but the resolution is remarkable. Meanwhile, Prego et al. (2017) discovered that 2.3 GHz data enabled a more accurate outlying of the pipe signature for shallower pipes (less than 40 cm in depth), while 1 GHz and 800 MHz for deeper pipes.

2.4.1(g) Horizontal and vertical separation

The separation of two or more pipe signatures aligned vertically but at different depths is needed for an effective vertical resolution based on the antenna frequency. The hyperbolic reflections will overlap if the vertical spacing between these pipes is less than the vertical resolution given by the antenna frequency used, resulting in an incorrect interpretation (Prego et al., 2017). According to Prego et al. (2017), the 2.3 GHz frequency allowed pipes to be differentiated in vertical and horizontal directions with separations of around 10 and 25 cm, respectively but having a small penetration of 40 cm. The 1 GHz and 800 MHz frequencies, on the other hand, allowed for pipe signature separation with minimum horizontal and vertical separations of 50 and 20 cm, respectively. Meanwhile, the 500 MHz frequency did not have good pipe signatures due to poor resolution.

According to Rial et al. (2009), target reflections are strongly related to the transmitted pulse characteristics. A critical factor in conducting a successful GPR survey is having as much information about the antennas. As a result of the obtained data, it can be concluded that vertical resolution is not substantially affected by distance. The reflector composition influenced the vertical resolution, which generally increased with wooden bars. On the other hand, the metallic bar demonstrates that the tail of the reflected pulse in the first bar is sufficiently powerful to distort the second bar when the two are close together due to the metallic bars' higher RC. This effect is more pronounced in the results obtained with the 500 MHz antenna due to the longer pulse length. Vertical resolution is very similar for higher frequency antennas (1 GHz and 800 MHz) due to their central frequency and effective pulse duration similarity. Horizontal resolution worsens when reflectors are separated from antennas due to the increased footprint. When the bars are placed